

Critical analysis of the numerical setup for the Large Eddy Simulation of the low pressure turbine profile T106C

Christian Morsbach and Michael Bergmann

1 Introduction

The increasing availability of computational resources has led to numerous publications on large eddy and even sporadically on direct numerical simulations of low pressure turbine (LPT) flows with Reynolds numbers around 10^5 , e.g. [4, 11]. In need for an appropriate validation case, the community has focussed on the T106 profile series for which experimental data are publicly available [6]. The T106A and T106C variants at $Re = 60,000$ and $Re = 80,000$, respectively, at low inflow turbulence have been selected as an advanced test case in the *High-Order CFD Methods* workshop series. While the experiment was arranged as a linear cascade of six prismatic blades with an aspect ratio of 2.4, the computational geometry is simplified assuming pitchwise and spanwise periodicity and laminar inflow conditions. The spanwise domain size amounts to 10% of the chord length. Besides the influence of 3D effects, uncertainties exist concerning the exact inflow and stagger angles and have been addressed in several studies, cf. [4, 13]. Even if the nominal boundary conditions of the workshops are used, different numerical methods and solvers show a significant variation in the blade pressure distribution and wake loss profile [2, 3, 7].

In order to fairly assess advanced numerical methods such as high-order discretisation or synthetic turbulence inflow conditions, a good understanding of the numerical setup and its influence on the quantities of interest is required. In an LES, most of these are based on statistical moments. For practical reasons of available computing resources, these moments are estimated using a finite number of samples and are, hence, subject to statistical error. In order to be able to draw any meaningful conclusions when comparing two simulation results, this error has to be considered. Following this rationale, we performed a series of large eddy simulations of the

Christian Morsbach · Michael Bergmann
Numerical Methods, Institute of Propulsion Technology, German Aerospace Center (DLR), e-mail:
christian.morsbach@dlr.de

T106C LPT profile at isentropic exit conditions of $Re = 80,000$ and $M = 0.65$ using DLR's solver for turbomachinery flows TRACE and carefully analysed the results.

2 Numerical method

TRACE solves the filtered compressible Navier-Stokes equations using a second-order accurate, density based finite volume scheme applying MUSCL reconstruction with $\kappa = 1/3$ [5]. A fraction of 10^{-3} of Roe's numerical flux [10] is added to a central flux to avoid odd-even decoupling. Time integration is performed using a third-order accurate explicit Runge-Kutta method. The subgrid stresses are computed by the WALE model [8].

The following methods have been applied as boundary conditions:

Unsteady1DCharacteristics Time and surface average boundary state driven towards prescribed boundary values (stagnation pressure and temperature, flow angles at inflow, static pressure at outflow) by means of incoming characteristics. 1D non-reflecting. [12]

Riemann Time and space local state forced to meet prescribed boundary values (as above) based on Riemann invariants. Prone to reflections. [1]

Dirichlet Directly prescribe time and space local state computed with prescribed velocity vector and static temperature while static pressure is taken from inner cell. Reflecting.

If not otherwise stated, the 1D non-reflecting boundary condition is used for both inflow and outflow.

The primary data obtained from LES are time series of the filtered quantities at the solution points. In the following averaging process over a finite length sample, any filtered quantity f can be split into a time mean \bar{f} and a fluctuating part f' . The error on the mean is given by

$$\sigma_{\bar{f}} = \sqrt{\frac{\sigma_f^2}{n}}, \quad n = \frac{T_{\text{average}}}{2T_{\text{int}}}, \quad T_{\text{int}} = \int_0^\infty \frac{\overline{f'(t)f'(t+\tau)}}{\sigma_f^2} d\tau \quad (1)$$

with the variance σ_f^2 and the number of independent samples n . The latter can be estimated by relating the integral time scale T_{int} to the length of the averaging interval T_{average} [9]. A measure for the integral time scale can be obtained from the integral over the auto-correlation function. For practical reasons, the integral is truncated at the first zero crossing of the integrand.

Errors on the derived quantities of engineering interest are obtained using error propagation. The isentropic Mach number and total pressure loss coefficient are given by

$$\overline{M}_{\text{is}} = \sqrt{\frac{2}{\gamma-1} \left(\left(\frac{\overline{p}_t^{\text{ref}}}{\overline{p}} \right)^{\frac{\gamma-1}{\gamma}} - 1 \right)}, \quad \overline{\zeta} = 1 - \frac{\overline{p}_t}{\overline{p}_t^{\text{ref}}} \quad (2)$$

with the heat capacity ratio γ , reference stagnation pressure p_t^{ref} , stagnation pressure p_t and static pressure p treated as independent variables.

Results of the grid study are not reported due to space constraints. The final grid was resolved with 40 points per 10% chord in spanwise direction, giving a total of $10.723 \cdot 10^6$ cells with non-dimensional cell sizes of $\Delta x_{\text{max}}^+ = 40.5$, $\Delta x_{\text{avg}}^+ = 9.0$, $\Delta z_{\text{max}}^+ = 24.6$, $\Delta z_{\text{avg}}^+ = 8.6$ and $y^+ < 0.91$ along the blade surface.

3 Results and discussion

The flow field was initialised using a RANS solution from which the simulation shows a transient phase of 2D vortex shedding. Eventually, the vortices break down into turbulent structures. All times are expressed in terms of the convective time $T_{\text{through}} = c/u_{\text{exit}}$ with a chord length $c = 0.093$ m and an approximate exit velocity $u_{\text{exit}} \approx 200$ m/s. A quantity to assess the passing of the initial transient is the blade force F_y , averaged over 10 throughflows normalised by the average over the last 90 throughflows as shown in Fig. 1 (*left*). It can be said that the initial transient has washed out after about 10 throughflows.

Fig. 1 (*right*) shows the statistical convergence of the mean total pressure loss coefficient ζ and its error σ_ζ with increasing averaging time t_{av} . Each line corresponds to a different pitchwise position traversing the pressure side of the wake at $x = x_{\text{TE}} + 0.7c_{\text{ax}}$ with the axial position of the trailing edge x_{TE} and the axial chord length c_{ax} . Even after 90 throughflows, some drift can be observed especially in the centre of the wake. It remains, however, within the statistical error. Due to limited computational resources, the following studies were conducted with averages over 90 throughflows.

The choice of inflow boundary condition formulation revealed a significant influence on the blade pressure distribution. It has to be mentioned that RANS simulations are basically insensitive to this choice for this case, hence, the effect must be due to unsteady reflections of upstream travelling waves. Fig. 2 (*left*) shows the blade pressure distribution in terms of isentropic Mach number. The locations at which probe data were available to estimate the error are marked with crosses. Only within this range is the error indicated by shaded regions. The three methods produce significantly different results downstream of the suction side separation point. The results obtained with the *Dirichlet* boundary condition are characterised by a very thin closed separation bubble while. Changing to the *Riemann* formulation with the inlet 0.1 m away from the leading edge thickens the still closed separation bubble. Moving the inlet upstream to 0.2 m to weaken the influence of reflections or employing the 1D non-reflecting formulation at 0.1 m leads to an open separation bubble and the best agreement with experiments. The great spread in the results sug-

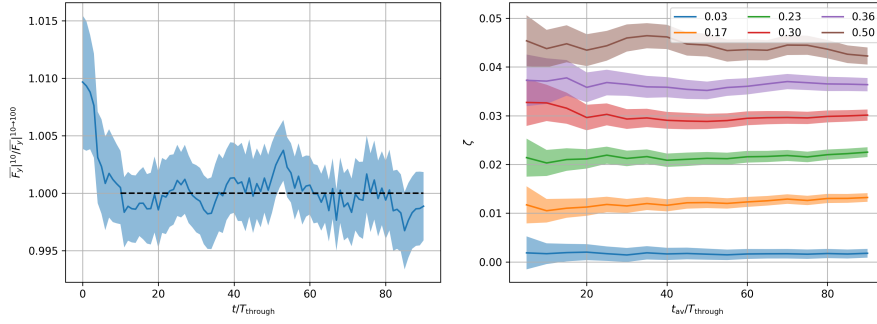


Fig. 1 Statistical convergence of pitchwise blade force averaged over 10 throughflows (*left*) and total pressure loss coefficient at $x = x_{\text{TE}} + 0.7c_{\text{ax}}$ at different relative pitchwise positions (*right*).

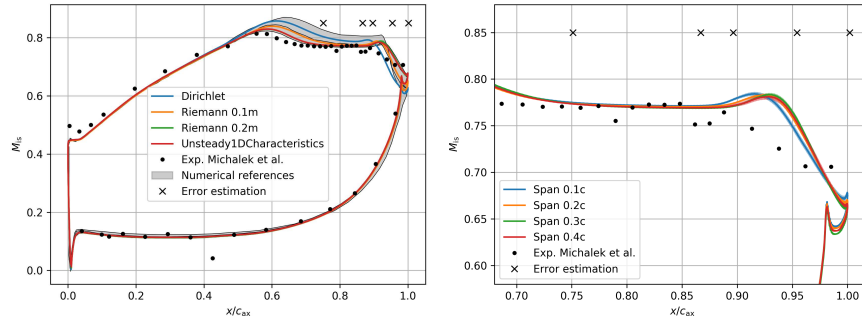


Fig. 2 Blade pressure distribution in terms of isentropic Mach number for different inflow boundary conditions with numerical references [2, 3, 7] (*left*) and spanwise domain sizes (*right*).

gests that most of the observed variations in the literature could be due to different formulations of boundary conditions.

At a first glance at Fig. 2 (*right*), the influence of the spanwise domain size is rather small yet statistically significant. The different pressure distribution can be attributed to a slight change in shape of the separation bubble, especially a small secondary recirculation region within the bubble at $x/c_{\text{ax}} \approx 0.9$. The differences become more obvious downstream in the wake. Fig. 3 is based on data from a 1D-probe near its centre at $x = x_{\text{TE}} + 0.4c_{\text{ax}}$. The normalised two-point correlation along the span is shown for the axial u' and spanwise w' component of the fluctuating velocity (*left*). For 10% span the latter reaches zero within half the domain size. With increasing domain size, the zero-crossing gradually moves to below a quarter. It has to be mentioned though, that the two-point correlation does not show a zero value for large Δz . For the axial velocity component, zero is not even reached for greater domains and a very high correlation value above 0.6 remains for 10% span. Looking at the raw time traces, this can be attributed to significant periods of spanwise fully correlated flow. To quantify this, an instantaneous turbulence intensity

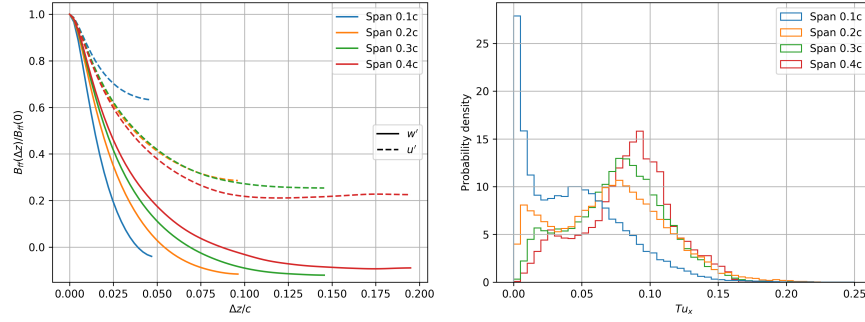


Fig. 3 Two-point correlation of axial and spanwise velocity (*left*) and histogram of instantaneous turbulence intensity (*right*) at $x = x_{TE} + 0.4c_{ax}$ in the centre of the wake.

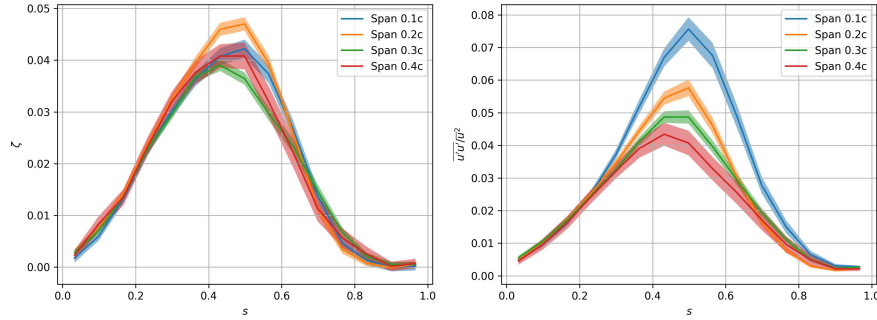


Fig. 4 Total pressure loss coefficient (*left*) and axial Reynolds stress component (*right*) at $x = x_{TE} + 0.7c_{ax}$.

$$Tu_x(t) = \frac{\sqrt{\langle u'^2(x,t) \rangle}}{\langle u(x,t) \rangle} \quad (3)$$

can be defined using a spanwise average denoted by $\langle \cdot \rangle$. The probability density distribution of this quantity is shown in Fig. 3 (*right*). For every span, we observe a distribution with two peaks - one at low and one at high turbulence intensity. The anomalous peak at 0 can be seen as a hint for too small a spanwise domain. Increasing the span significantly changes the distribution towards a state where no fully correlated phases across the span exist. Therefore, the assumption of spanwise periodicity in combination with too small domain sizes can lead to wrong conclusions.

The total pressure loss wake profile in Fig. 4 (*left*) shows an oscillatory dependence on the domain size while the axial Reynolds stress component (*right*) decreases with increasing domain size. Both quantities show a statistically significant influence of the domain size. For this case we conclude, that the domain should cover at least $0.3c$.

4 Conclusion

The numerical setup of an LES of the T106C LPT profile has been assessed considering the statistical error on mean values due to finite averaging times. Both inflow boundary conditions and the spanwise domain size show a significant influence on the predicted blade pressure distribution and wake profiles. Most of the variation of numerical results for the pressure distribution can be attributed to the choice of inflow boundary condition. For the considered Reynolds number of 80,000, typically assumed spanwise domain sizes of $0.1c$ are insufficient to capture the decay of 2D structures into turbulence appropriately.

References

- [1] Carlson, J.R.: Inflow/outflow boundary conditions with application to FUN3D. Tech. Rep. NASA TM-2011-217181, NASA Langley Research Center (2011)
- [2] Garai, A., Diosady, L.T., Murman, S.M., Madavan, N.K.: DNS of low-pressure turbine cascade flows with elevated inflow turbulence using a discontinuous-Galerkin spectral-element method. In: ASME Turbo Expo. Seoul, Korea (2016)
- [3] Hillewaert, K., Hartmann, R., Leicht, T., Couaillier, V., Wang, Z.J., Cagnone, J.S.: Summary and conclusions of the 4th international workshop on high order CFD methods. In: ECCOMAS. Crete, Greece (2016). URL <https://how4.cenaero.be/content/ms910-eccomas-cfd-2016>
- [4] Hillewaert, K., Carton de Wiart, C., Verheylewegan, G., Arts, T.: Assessment of a high-order discontinuous Galerkin method for the direct numerical simulation of transition at low-reynolds number in the T106C high-lift low pressure turbine cascade. In: ASME Turbo Expo. Düsseldorf, Germany (2014)
- [5] van Leer, B.: Towards the ultimate conservative difference scheme. V. A second-order sequel to Godunov's method. *J. Comput. Phys.* **32**(1), 101 – 136 (1979)
- [6] Michálek, J., Monaldi, M., Arts, T.: Aerodynamic performance of a very high lift low pressure turbine airfoil (T106C) at low Reynolds and high Mach number with effect of free stream turbulence intensity. *J. Turbomach.* **134**(6) (2012)
- [7] Mitra, P., Mathew, J.: Large eddy simulation of turbine aerodynamics by explicit filtering. In: GPPS Montreal18 Proceedings. Montreal, Canada (2018)
- [8] Nicoud, F., Ducros, F.: Subgrid-scale stress modelling based on the square of the velocity gradient tensor. *Flow Turbul. Combust.* **62**(3), 183–200 (1999)
- [9] Ries, F., Nishad, K., Dressler, L., Janicka, J., Sadiki, A.: Evaluating large eddy simulation results based on error analysis. *Theor. Comp. Fluid Dyn.* **32**(6), 733–752 (2018)
- [10] Roe, P.L.: Approximate Riemann solvers, parameter vectors, and difference schemes. *J. Comput. Phys.* **43**(2), 357 – 372 (1981)
- [11] Sandberg, R.D., Michelassi, V., Pichler, R., Chen, L., Johnstone, R.: Compressible direct numerical simulation of low-pressure turbines—part I: Methodology. *J. Turbomach.* **137**(5) (2015)
- [12] Schluß, D., Frey, C., Ashcroft, G.: Consistent non-reflecting boundary conditions for both steady and unsteady flow simulations in turbomachinery applications. In: ECCOMAS. Crete, Greece (2016)
- [13] Carton de Wiart, C., Hillewaert, K., Lorriaux, E., Verheylewegan, G.: Development of a discontinuous Galerkin solver for high quality wall-resolved/modelled DNS and LES of practical turbomachinery flows on fully unstructured meshes. In: ASME Turbo Expo. Montreal, Quebec, Canada (2015)